PERGAMON

Applied Radiation and Isotopes 50 (1999) 343–353

Applied Radiation and Isotopes

Measurements of discrete and continuous X-ray spectra with a photodiode at room temperature

Ricardo A. Terini [a,*], Paulo R. Costa [b], Tânia A.C. Furquim [b], Silvio B. Herdade [c]

[a] *Departamento de Física, Pontifícia Universidade Católica de São Paulo, R. Marquês de Paranaguá, 111, 01303-050, São Paulo, SP, Brazil*

[b] *Instituto de Eletrotécnica e Energia, Universidade de São Paulo, Av. Prof. Luciano Gualberto, 1289, 05508-900, São Paulo, SP, Brazil*

[c] *Instituto de Física, Universidade de São Paulo, Caixa Postal 66318, 05389-970, São Paulo, SP, Brazil*

Received 17 June 1997; accepted 24 October 1997

Abstract

Spectra of X- and γ-rays emitted by radioactive sources and of the radiation emitted by X-ray tubes, in the energy range 15–160 keV, have been measured with a silicon PIN photodiode at room temperature. The experimental X-ray tube spectra are compared with calculated ones on the basis of a semi-empirical model. Results indicate that the method utilized is adequate for the characterization of X-ray beams in the medical diagnostic energy region.

1. Introduction

Silicon PIN photodiodes, in nuclear spectroscopic measurements, are mainly used for the detection of light from scintillators (Suffert, 1992). This combination offers several advantages as compared to photomultiplier tube-scintillator assembly as large quantum efficiency, no gain drifts in magnetic fields, low operating voltages and power consumption, as well as low cost. Due to their extremely low leakage currents (down to a few nA) and low noise, silicon PIN photodiodes have been used to measure X-and γ-rays directly. Furthermore, because of the low average energy (3.6 eV) required to create an electron–hole pair in the depletion layer of silicon, ionizing radiation creates a large number of charge carriers in a small volume. Thus, the statistical contribution to the peak-width of the energy spectra is much less for these detectors than it would be for scintillation detectors. PIN photodiodes with low capacitance even with large areas are now available, and their energy resolution has been reduced in the last ten years with the use of special designed devices and preamplifiers, as well as by cooling. Photodiodes with small active areas present a resolution of 1.2–2.0 keV at room temperature (Aoki and Koyama, 1989; Yamamoto et al., 1989; Ahmad et al., 1990; Gramsch et al., 1992) measured by the peak's full width at half maximum (FWHM). This resolution can be compared to that of cooled Si(L1) detectors coupled to preamplifiers with cooled FET, which is in the range 0.6–0.8 keV (Ahmad and Wagner, 1979). Therefore, PIN photodiodes become competitive even for high resolution photon spectroscopy in the keV energy region.

On the other hand, the knowledge of the X-ray spectra is very important in many applications as, for example, in medical diagnostic radiology and in radiation dosimetry. This knowledge leads to patient dose reduction in radiological examinations and to optimize image quality in image receptors (Seelentag and Panzer, 1979; Pani et al., 1987; Aoki and Koyama, 1989). The characterization of a X-ray beam is also important to achieve spectral conformance with radi-

* To whom all correspondence should be addressed.

0969-8043/99/$ - see front matter
PII: S0969-8043(97)10123-3

ation emitters of different laboratories and to allow intercomparison of test results.

Measurements of medical diagnostic X-ray spectra have been reported by several authors, using different detectors: NaI(Tl) (Epp and Weiss, 1966), Ge(Li) or Si(Li) (Israel et al., 1971; Fewell and Shuping, 1977; Seelentag and Panzer, 1979; O'Foghludha and Johnson, 1981), and surface barrier detectors (Pani et al., 1987). A comparison reveals large differences amongst the spectra obtained with such detectors. Ge or Si (L1) have been more frequently used for accurate spectral measurements, with proper corrections (Fewell and Shuping, 1977; Seelentag and Panzer, 1979). However, there are some disadvantages in using these systems: in measurements with medical X-ray equipment, it is necessary to decrease the count rate by using a pinhole collimator and to reduce the leakage current of the detector by cooling. With this collimation it is impossible to measure photons with different incident angles simultaneously, and hence, scattered radiation. Furthermore, the large liquid nitrogen container is inconvenient for certain applications, and there are additional difficulties of working with high voltages.

Recently, a few papers have reported the use of PIN photodiodes for spectrometry of diagnostic X-rays (Aoki and Koyama, 1989, 1990). These small area junction devices combine low operating voltages, low leakage current and attractive cost, with good resolution even at room temperature. Thus, X-ray spectra can be measured without cooling when one doesn't wish extremely high resolution, which is the case in some applications. Although the detection efficiency for X-rays is extremely limited, this characteristic makes it possible to measure incident X-ray spectra without pinhole collimators. Due to their small dimensions, most of commercial PIN photodiodes can be easily utilized in measurements of primary radiation or inside phantoms.

This paper presents some new measurements of discrete and continuous photon spectra, in the energy range 15–160 keV, with a photodiode at room temperature. The raw data are corrected by means of a stripping procedure which takes into account the photodiode full-energy absorption efficiency as a function of photon energy. Measured spectra of X-ray equipments are compared with spectra calculated on the basis of a semi-empirical model — the TBC model (Tucker et al., 1991).

2. Experimental method

The detector used for X-ray measurements was a Siemens SFH 206 K silicon planar PIN photodiode, with a nominal sensitive area of 7.0 mm^2. The square silicon chip is housed in a colorless transparent plastic package with a thickness of 1.3 mm over the sensitive area. This plastic window was reduced to 0.7 mm in order to reduce X-ray absorption. The capacitance of the photodiode was (8.5 ± 0.6) pF, with the reverse bias of 30 V used in the measurements. The depletion layer thickness, determined from the area and capacitance of the p–n junction, assuming a parallel plate geometry, was (88 ± 6) μm. The photodiode leads were soldered directly to a coaxial cable, with a SHV connector in the opposite end, forming a small probe 5.0 cm in length. To avoid the exposure of the photodiode to light, the probe was first covered with a (0.38 ± 0.01) mm thick black PVC thermoshrink wrapping. This wrapping was then covered with a thin (3.2 mg/cm^2) aluminium foil which served as an electrical shield. Some of the measurements were made without the PVC cover, but with two layers of the aluminium foil.

The electronic system utilized for the measurements consisted of an Ortec 456 HV power supply, an Ortec 142 IH preamplifier, an Ortec 572 amplifier, a Northern NS 623 ADC, and a microcomputer adapted to operate as a multichannel analyzer. All the measurements have been carried out with the photodiode and preamplifier at room temperature.

Spectra of X- and γ-rays emitted by the radioactive sources ^{241}Am, ^{109}Cd, ^{133}Ba and ^{152}Eu, with activities between 10^4 and 10^5 Bq, have been measured. The sources were placed at a distance of 2 cm from the photodiode. These discrete spectra were used to calibrate the X-ray spectrometer, which resulted in linear energy vs channel number curves, and to determine the energy resolution and full-energy efficiency of the photodiode. The full width at half maximum (FWHM) for the peaks of the measured source spectra, in the energy range 13–122 keV, are presented in Table 1.

Continuous spectra of X-ray tubes, with electron acceleration voltages ranging from 60 to 160 kV, were obtained using the following equipment: (a) a Philips MCN 421 water cooled X-ray tube, with a tungsten target at an angle of 30°, 2 mm beryllium window, connected to a Philips MG 450 system with a constant potential generator stabilized within 0.3%, and 0.10 mA current in the tube; (b) a Rörix X-ray tube having a rotating tungsten/rhenium target with an angle of 17.5° and inherent filtration equivalent to 1.7 mm Al, connected either to a system with a three-phase generator (with a ripple of ~10%) or to a Siemens Heliophos 4B single-phase apparatus operating in the fluoroscopic mode (ripple ~2%), both with currents less than 2 mA. The focal spot-photodiode detector distance was 2.8 m for the Philips MCN 421 tube, and 1.50 m for the Rörix tube (with a Pb collimator).

Table 1
Full width at half maximum (FWHM) of the peaks obtained in the spectral measurements with radioactive sources

Source	Peak energy (keV)*	FWHM (keV)
^{241}Am	13.927	3.4
^{241}Am	17.611	3.4
^{109}Cd	22.163	3.9
^{241}Am	26.344	2.5
^{133}Ba	30.973	4.1
^{152}Eu	40.118	4.1
^{133}Ba	53.148	2.9
^{241}Am	59.536	4.0
^{133}Ba	80.989	4.0
^{109}Cd	88.034	3.6
^{152}Eu	121.776	4.2

*Browne and Firestone (1986).

3. Spectral corrections and data analysis

3.1. Photodiode efficiency for photon total energy absorption

Commercially available PIN Si photodiodes have, in general, a small sensitive layer thickness ($< 100\ \mu$m), as compared to Si(Li), Ge(Li) or HP Ge detectors. Due to this thin depletion layer, the efficiency for the detection of X-ray photons presents a strong energy dependence. In the present work, the efficiency of the Siemens SFH 206K photodiode, for photon total energy absorption in the diagnostic range, have been calculated and experimentally determined. As the volume of the *i*-layer is very small, the incident photons rarely suffer multiple interactions (less than 1% of the total). Then we may assume that the total energy photon absorption in Si occurs only by photoelectric effect, and the partial absorption only by Compton scattering.

The efficiency for the photoelectric effect may be calculated by

$$\eta_p = (\mu_p/\mu_t)(1 - e^{-(\mu_t/\rho)t}) \quad (1)$$

where μ_p and μ_t are the photoelectric and total linear attenuation coefficients for Si in cm^{-1}, respectively (Storm and Israel, 1970), ρ is the Si density in g/cm^3 and t is the depletion layer thickness (in g/cm^2). The *K*-escape may be also ignored in this case due to the low energy of the *K*-edge for Si (1.84 keV) and the low probability for fluorescence (0.05). On the other side, for a Si photodiode, the escape of photoelectrons must be considered, since the extrapolated range of 100 keV electrons in silicon is 58 μm, very close to the thickness of the depletion layer of 88 μm. The data presented by Aoki and Koyama (1989) have been used to determine the fraction, f_e, of photoelectrons that escape from the silicon *i*-layer after the photon interaction. In this determination, only the frontal scattering probability of the photoelectrons, after a photon interaction with a Si atom, is considered. The efficiency for total energy absorption, corrected for the escape of photoelectrons, will then be given by

$$\eta_f = \eta_p(1 - f_e) \quad (2)$$

For the measurements carried out in the present work, it was still necessary to correct η_f for the attenuation of the photon beam in the materials between the X-ray source and the sensitive layer of the photodiode, namely the dead Si p^+ layer ($\leq 1\ \mu$m) (Sakai, 1987; Gramsch et al., 1992), the photodiode plastic wrapping, the black PVC thermoshrink wrapping, the Al foil electrical shield, and air. Thus, the efficiency η_f', corrected for the attenuation in these materials is given by

$$\eta_f' = \eta_f \cdot f_d \quad (3)$$

where f_d is the product of the absorption factors related to each one of the considered materials.

The calculated efficiency η_f', using Eq. (3), for several energies of X- and γ-rays emitted by ^{109}Cd, ^{133}Ba, and ^{152}Eu, sources are presented in Table 2. Also shown are experimental data obtained from the ratio of measured full-energy peak counting rates to the respective published emission rates (Rens and Westmeier, 1983), after correction of these last rates for the absorption in the radioactive source covers. The experimental efficiencies $\eta_{f,exp}$ are normalized to the calculated η_f' values at 88.034 keV (for ^{109}Cd), 30.625/30.973 keV (for ^{133}Ba), and 121.77 keV (for ^{152}Eu). Fig. 1 shows η_f' and $\eta_{f,exp}$ vs photon energy in the energy range covered in the present work.

3.2. Correction (stripping) of the experimental obtained spectra

In order to correct the experimental data to obtain the original radiation spectrum, a microcomputer program (Stripping 2.0) has been developed in Mathcad (Mathsoft). Such program takes into account the efficiency for total energy absorption, the Compton scattering, the radiation scattered by the metallic components of the photodiode, and the attenuation of the incident beam by the materials located between the radiation source and the sensitive region of the detector. A flowchart of this program is presented in Appendix A.

After reading of the files containing the experimental data corresponding to measurements with and without the radiation source (noise), the program initiates the net counting correction starting from the last channel. The measured data are then corrected for the photo-

Table 2
Efficiency η_f', as calculated by Eq. (3) and normalized experimental data $\eta_{f,\mathrm{exp}}$ (see text)

Source	Energy (keV)	η_f'	$\eta_{f,\mathrm{exp}}$
^{109}Cd	21.990/22.163	4.32×10^{-2}	$(4.75 \pm 0.25) \times 10^{-2}$
	24.934/25.603	3.08×10^{-2}	$(3.34 \pm 0.19) \times 10^{-2}$
	88.034	6.30×10^{-4}	6.30×10^{-4}
^{133}Ba	30.625/30.973	1.84×10^{-2}	1.84×10^{-2}
	34.967/36.006	1.25×10^{-2}	$(1.11 \pm 0.02) \times 10^{-2}$
	53.148	3.38×10^{-3}	$(2.76 \pm 0.57) \times 10^{-3}$
	79.612/80.989	8.52×10^{-4}	$(8.93 \pm 0.54) \times 10^{-4}$
^{152}Eu	39.522/40.118	8.42×10^{-3}	$(8.0 \pm 2.6) \times 10^{-3}$
	45.379/46.819	5.53×10^{-3}	$(5.7 \pm 1.9) \times 10^{-3}$
	121.77	1.93×10^{-4}	1.93×10^{-4}

diode efficiency, calculated by Eq. (3) and presented in Table 2 and Fig. 1.

Values for the attenuation coefficients of Si and materials between the radiation source and the sensitive layer of the photodiode have been calculated using a least square fit to the data obtained in the literature (Storm and Israel, 1970; Hubbel, 1982).

The distortion due to Compton scattering is corrected by assuming a rectangular shape approximation for the scattered spectrum below the Compton-edge (Seelentag and Panzer, 1979; Aoki and Koyama, 1989). The efficiency for Compton scattering is given by

$$\eta_c = (\mu_c/\mu_t)[1 - e^{-(\mu_t/\rho)t}] \quad (4)$$

where μ_c and μ_t are the linear attenuation coefficients in Si for Compton scattering and total energy absorption, respectively, ρ is the Si density and t is the thickness of the depletion region. It is not necessary to take into account the escape of the recoil electrons, since their range in silicon is much smaller than the depletion layer ($\sim$6 μm for 28 keV electrons produced by 100 keV photons). For the correction, the average counting per channel in the Compton continuum h (the rectangle height) is finally subtracted in the region from channel 1 to channel c, corresponding to the Compton-edge. This average counting h may be determined by the expression

$$hc = \eta_c N_T \quad (5)$$

where η_c is the efficiency for Compton scattering given by Eq. (4), and N_T is the corrected counting in the peak corresponding to the total energy of related photons. Such a procedure is carried out channel by

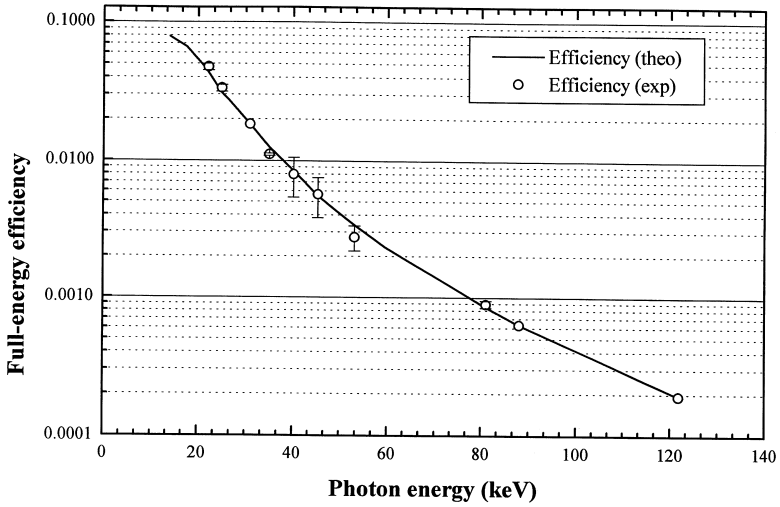

Fig. 1. Full-energy absorption efficiency η_f' and $\eta_{f,\mathrm{exp}}$ vs photon energy for the SFH 206K photodiode. The solid line represents the calculated η_f' and the circles with error bars correspond to the experimental $\eta_{f,\mathrm{exp}}$ data of Table 2. Error bars are related only to the least square fits to the spectral peaks.

channel, beginning also in the last and ending in the first channel.

There is also the necessity to correct the measured spectra for the radiation scattered by the metallic components of the photodiode. The Si wafer of the Siemens SFH 206K photodiode is mounted on a metallic contact of silver and indium. Such metallic layer may scatter photons that did not interact with the depletion layer of the Si wafer. For instance, the photons backscattered at 180° by Compton effect, occurred with 59.5 keV incident photons from ^{241}Am, have an energy of 48.2 keV. Photoelectrons which escape from this metallic contact may also reach the sensitive layer of the Si wafer. In our case, the experimental data were corrected for the scattered radiation by utilizing counts obtained with spectra of the radioactive sources ^{241}Am, ^{133}Ba, and ^{109}Cd, respectively, between the isolated peaks of 59.54, 80.99, and 88.03 keV, and the peaks immediately lower in energy, for each case. For the respective correction, such counts were supposed to be constant from zero to the channel corresponding to the energy of the photons that have caused the scattered radiation. The ratio F of the integral of the "scattered" counts to the integral of the photoelectric peak counts is energy dependent; such dependence has been determined by a linear regression of the values obtained from a curve of F as a function of the photon energy. The fraction F of the "scattered" counts is then subtracted from the measured counts in each channel.

Besides the radiation scattered by the metallic contact, photoelectric interactions in Ag and In will produce secondary (fluorescence) X-rays that will also be detected in the Si depletion layer, resulting in an additional spectrum superimposed on the spectrum of interest. The characteristic K X-rays of silver have energies of 21.99, 22.16, 24.93, and 25.43 keV, and those of indium 24.00, 24.21, 27.27, and 27.86 keV. The correction taking into account these fluorescence X-rays is particularly difficult. Other photodiodes may or may not need this correction, depending on the fabrication process. In the present work, the correction for the Ag characteristic K X-rays, the major contribution to this fluorescence, has been carried out by utilizing the spectrum of the ^{109}Cd source, previously measured; this nuclide decays to an isotope of Ag which emits its characteristic X-rays. Thus, by an appropriate subtraction of this Cd spectrum from the measured data, in the range 0–30 keV, the superimposed Ag K X-ray contribution can be eliminated.

3.3. Calculation of semi-empirical spectra based on TBC model

The model proposed by Tucker et al. (1991) (TBC model) presents different formulations for the evaluation of both continuum spectra (*Bremsstrahlung*) and characteristic lines emitted by an X-ray tube. The model considers the target material and attenuation, the geometry of the anode and the attenuation by the tube window and added filtration. The proposed equation for the Bremsstrahlung was

$$N(E)\mathrm{d}E = \frac{\alpha \cdot r_e^2 \cdot Z^2}{A}\frac{\mathrm{d}E}{E}\int_E^{T_0}\frac{B(T+m_0c^2)}{T}F(E,\,T)\cdot \left(\frac{1}{\rho}\frac{\mathrm{d}T}{\mathrm{d}x}\right)^{-1}\mathrm{d}T \tag{6}$$

where: α is the fine structure constant; r_e is the classical electron radius; m_0 is the rest mass of the electron; c is the velocity of light; Z and A are the effective atomic number and the mass of the target atoms, respectively. T_0 is the initial kinetic energy of the electrons; T is the kinetic energy of the electrons inside the target; $(1/\rho)(\mathrm{d}T/\mathrm{d}x)$ is the mass stopping power of the target atoms; B is a function proportional to the number of X-ray photons emitted per electron, and

$$\begin{aligned} F(E,\,T) &= \exp[-\mu_{\mathrm{WR}}(E)\cdot d] = \exp[-\mu_{\mathrm{WR}}(E)\cdot x/\mathrm{sen}\,\theta] \\ &= \exp[-\mu_{\mathrm{WR}}(E)\cdot (T_0^2 - T^2)/(\rho C\,\mathrm{sen}\,\theta)] \end{aligned} \tag{7}$$

where $\mu_{\mathrm{WR}}(E)$ is the linear attenuation coefficient of the target material for an X-ray of energy E; θ is the target angle; and $C = (T_0^2 - T^2)/\rho x$ is the Thomson–Widdington constant.

The model considers a parabolic probability distribution function in order to account for the characteristic emission by the target material. This distribution appears as a function of the distance x travelled by the electrons inside the anode and was modeled as

$$P\left(\frac{x}{R}\right) = \begin{cases} \cdot\left(\frac{3}{2}\right)\left[1 - \left(\frac{x}{R}\right)^2\right], & x \le R \\ \cdot 0, & x > R \end{cases} \tag{8}$$

where R is the distance at which the average kinetic energy of the electrons is equal to the K-shell binding energy. By using this function, the characteristic emission can be calculated by

$$N(E_i) = A_k\left(\frac{T_0}{E_k} - 1\right)^{n_k} f(E_i)\int_0^R P \left(\frac{x}{R}\right)\mathrm{e}^{-\mu_{WR}(E_i)x/sen\,\theta}\mathrm{d}x \tag{9}$$

where A_k and n_k are model parameters and $f(E_i)$ is the fractional emission for the characteristic energy E_i.

A routine for implementing the equations above were developed also by using the Mathcad software. Both model parameters and parametrized equations for the mass stopping power and for the function B followed the indications included in the Tucker *et al.* paper. Values of the Thomson–Widdington constant were provided for electron incident energies of 50, 75, 100, 150 and 200 keV. These values were interpolated by using the spline fitting routine included in the Mathcad package, in order to provide a continuous grid for calculating the X-ray spectra. Results of a computer simulation of 60, 73, 100 and 160 kVp spectra by using this methodology are presented in Figs. 4–7.

4. Results and discussion

The measured X- and γ-ray spectra are presented in Figs. 2–7. The raw data have been corrected by the procedure described previously. The measured and corrected spectra of ^{241}Am and ^{133}Ba are presented in Figs. 2 and 3, respectively; the circles are experimental data and the solid lines have been drawn just to guide the eye. The fluorescent Ag K X-ray peak is not observed in the ^{241}Am spectrum [Fig. 2(a)] because it is masked by the low energy peaks of this nuclide. The values for the full width at half maximum (FWHM) of the peaks are presented in Table 1. The relative intensities of peaks in the measured

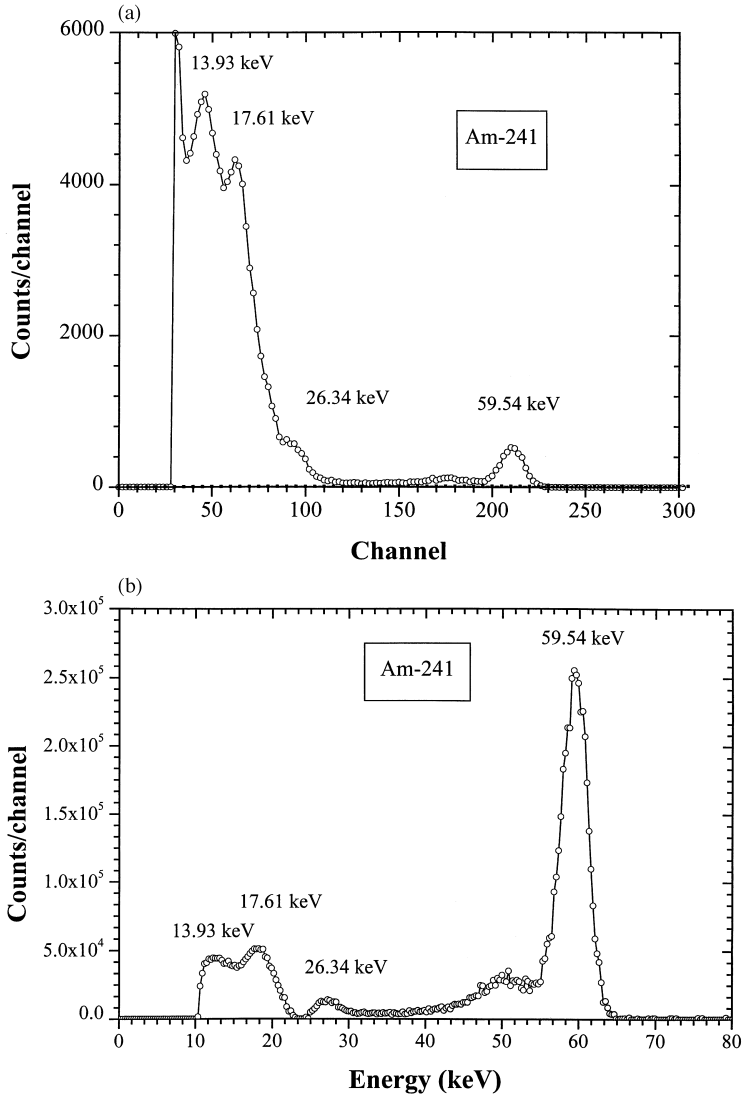

Fig. 2. (a) Measured X- and γ-ray spectrum of ^{241}Am. (b) Corrected X- and γ-ray spectrum of ^{241}Am. The peak at about 50 keV corresponds to photon back scattering due to the silver layer in the photodiode.

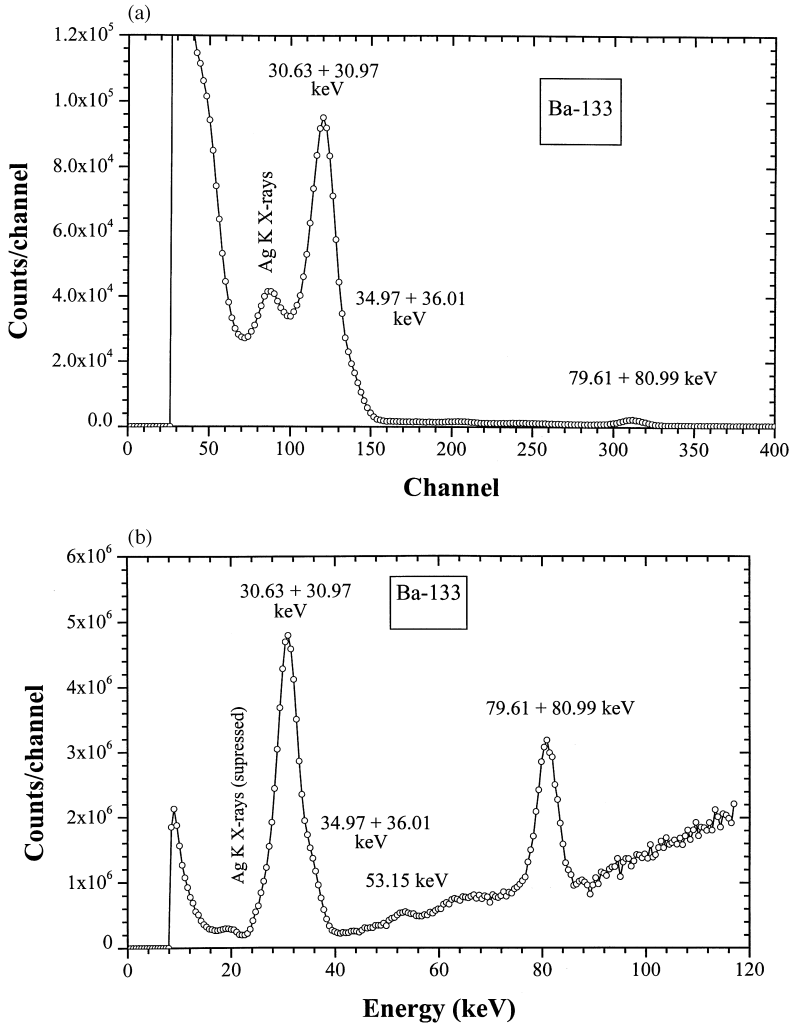

Fig. 3. (a) Measured X- and γ-ray spectrum of ^{133}Ba. (b) Corrected X- and γ-ray spectrum of ^{133}Ba.

photon spectra have been determined and compared with corresponding data published in the literature (Browne and Firestone, 1986). The result of this comparison is presented in Table 3, showing a good agreement.

The measured and corrected spectra of beams emitted by X-ray tubes are presented in Figs. 4–7. Fig. 4(a) presents the measured spectrum (raw data) for the beam of the Philips MCN 421 tube described previously, with a constant potential of 160 kV, current

Table 3
Ratios of peak intensities R, obtained from the measured radioactive source photon spectra (after stripping), as compared to the corresponding ratios RL taken from the literature, for ^{241}Am and ^{133}Ba

Source	A_1	A_2	$R = A_1/A_2$	RL
^{241}Am	6.468×10^4 counts (26.3 keV)	1.138×10^6 counts (59.54 keV)	0.057	0.056
^{133}Ba	2.811×107 counts (30.625/30.973 + 34.967/36.006) keV	9.340×106 counts (79.612/80.989) keV	3.01	2.97

A_1: area under the first peak (counts); A_2: area under the second peak (counts); $R = A_1/A_2$: ratio of the peak intensities (areas), after stripping; RL: ratio of the peak intensities taken from the literature (Browne and Firestone, 1986), corrected for absorption in the source covers (0.22 mm of polyethylene + 0.52 mm of Al).

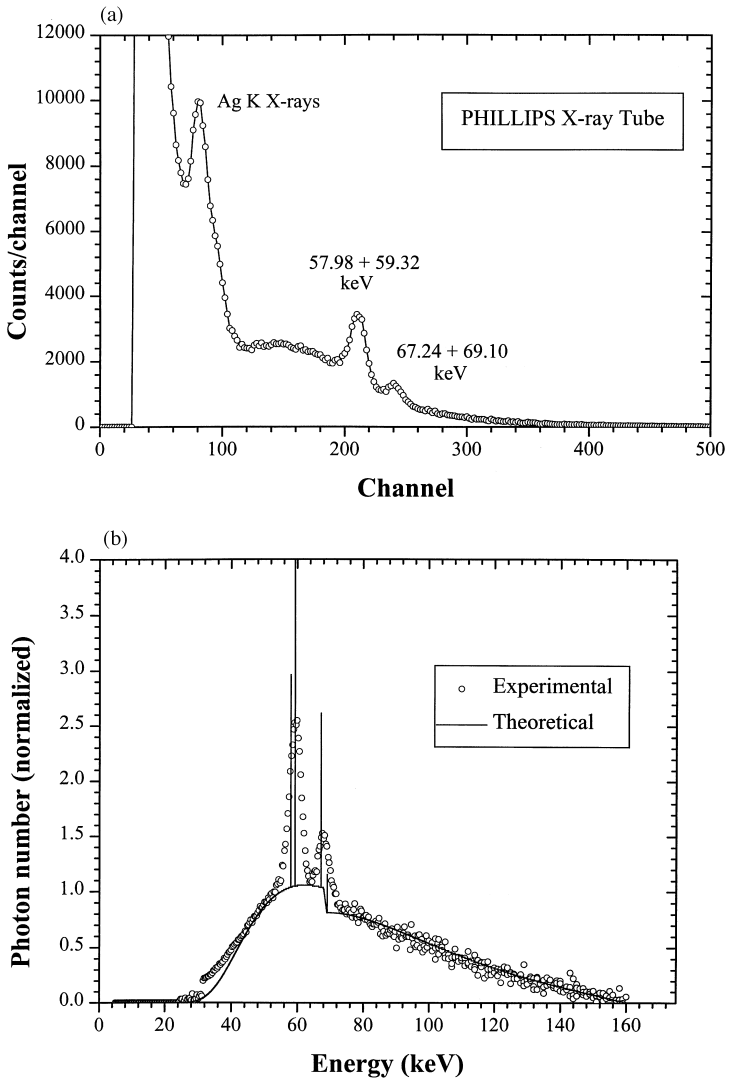

Fig. 4. (a) Measured X-ray spectrum of the beam emitted by the Philips MCN 421 tube (constant potential of 160 kV). (b) Comparison of the corrected experimental spectrum of (a) (circles) with the TBC model calculated spectrum (solid line). The data have been normalized at the maximum of the Bremsstrahlung spectrum; the vertical lines in the theoretical spectrum correspond to the tungsten characteristic X-rays (see text for details).

of 0.10 mA, and an additional filtration of 4.0 mm Al and 0.5 mm Cu. The corrected spectrum corresponding to the one shown in Fig. 4(a) is presented in Fig. 4(b). In this figure, the circles are the corrected experimental data and the solid line corresponds to the calculated spectrum on the basis of the TBC model. The experimental and theoretical data were normalized in the maximum of the Bremsstrahlung (continuous) spectrum. The peaks observed in the experimental spectrum of Fig. 4(a), (b), correspond to the characteristic X-rays of the tungsten target. The agreement between the experimental and theoretical results is good for the continuous part of the spectrum. In the characteristic X-rays region, the agreement is not so good due to the different resolutions of the experimental and theoretical data. All the theoretical spectra, both for the Philips MCN 421 and Rörix X-ray tube, have been calculated with a resolution in the energy scale of 0.01 keV; therefore, the tungsten and rhenium characteristic X-ray appear as thin vertical lines in the spectra.

Figs. 5–7 present the comparison of the corrected experimental and theoretical (TBC model) spectra related to the beam of the Rörix X-ray tube described previously. The conditions were as follows: Fig. 5 — applied voltage of 60 kV, as supplied by the Heliophos 4B single-phase apparatus operating in the fluoroscopic

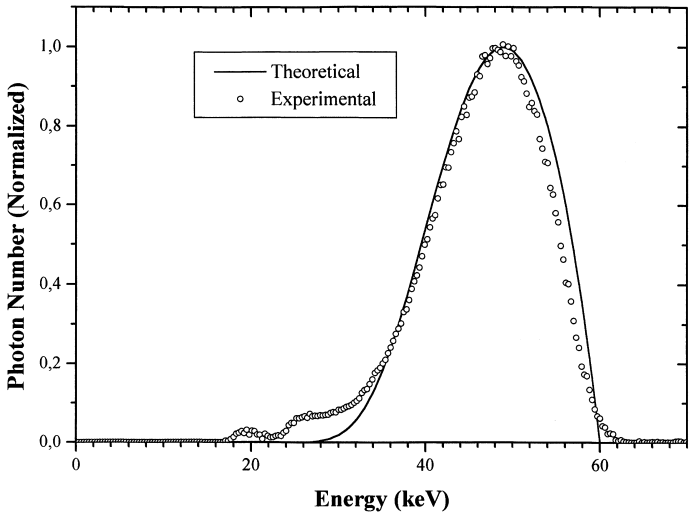

Fig. 5. Comparison of the corrected experimental (circles) and theoretical — TBC model (solid curve) spectra of the beam emitted by the Rörix X-ray tube; applied voltage of 60 kV (single-phase generator, fluoroscopic mode ~2% ripple); the vertical lines in the theoretical spectrum correspond to the tungsten and rhenium characteristic X-rays (see text for details).

mode (ripple ~2%), current ~2 mA, and an additional filtration of 3.4 mm Al and 0.6 mm Cu; Fig. 6 — applied voltage of 73 kV, as supplied by the same single-phase generator as in Fig. 5, and an additional filtration of 1.2 mm Al. Fig. 7 — applied voltage of 100 kV by the already described three-phase generator system, current ~2 mA, additional filtration of 4.7 mm Al. The vertical lines in the theoretical spectra of Figs. 5–7 refer to the tungsten and rhenium characteristic X-rays, whose energies are 57.98, 59.32, 67.24 and 69.10 keV for W, and 59.72, 61.14, 69.2 and 71.2 keV for Re. Fractional emissions have been calculated for an alloy with 90% of tungsten and 10% of rhenium atoms (Tucker et al., 1991).

The agreement between the experimental and theoretical spectra for the Rörix tube is reasonable but not so good as the one observed for the Philips MCN 421 tube. This is possibly due to the fact that the theoretical spectra have been calculated assuming a constant potential, and the Rörix tube has been operated with potentials with a percentage ripple greater than zero.

The present work has demonstrated that a simple detector, as a low cost photodiode at room tempera-

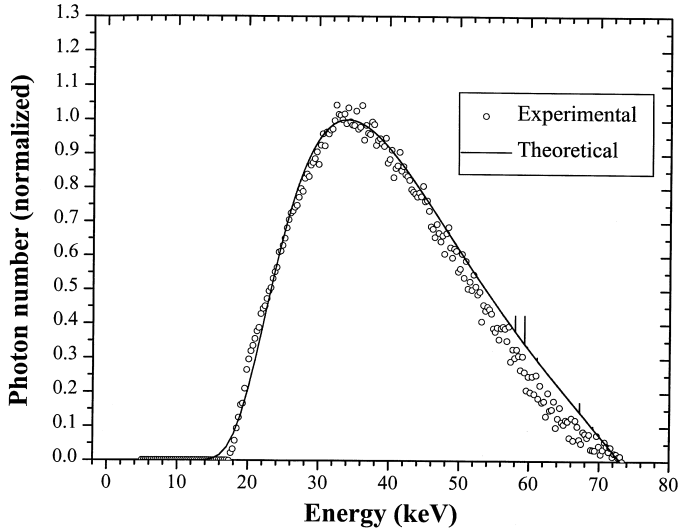

Fig. 6. Same as Fig. 5, for an applied voltage of 73 keV (see text for details).

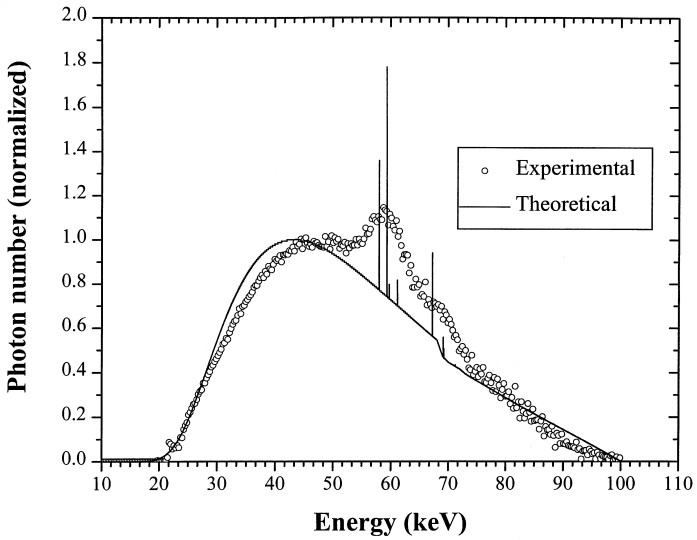

Fig. 7. Same as Fig. 5, for an applied voltage of 100 kV by a three-phase generator (ripple ~10%) (see text for details).

ture, is adequate for the measurement of X-ray tube spectra. The resolution of these detectors (3–4 keV) is sufficient to characterize the X-ray beams, whose spectra are dominated by the continuous Bremsstrahlung component. The comparison with calculated spectra supports this conclusion.

Acknowledgements

We would like to thank Dr. Marília Teixeira da Cruz for her assistance in the measurements with the Phillips X-ray tube, and Mr. Victor E. J. São Vicente for his help in developing the stripping program.

References

Ahmad, I., Wagner, F., 1979. A simple cooled Si(Li) electron spectrometer. Nucl. Instrum. Meth. 116, 465–469.

Ahmad, L., Betts, R. R., Happ, T., Henderson, D. J., Wolfs, F. L. H., Wuosman, A. H., 1990. Nuclear spectroscopy with Si PIN diode detectors at room temperature. Nucl. Intrum. Meth. A 299, 201–204.

Aoki, K., Koyama, M., 1989. Measurement of diagnostic X-ray spectra using a silicon photodiode. Med. Phys. 16, 529–536.

Aoki, K., Koyama, M., 1990. A silicon diode in a thimble-type mount for measurement of diagnostic X-ray spectra. Phys. Med. Biol. 35, 105–1517.

Browne, E., Firestone, R. B., 1986. In: Shirley, V. (Ed.), Table of Radioactive Isotopes. John Wiley and Sons.

Epp, E. R., Weiss, H., 1966. Experimental study of photon energy spectrum of primary diagnostic X-rays. Phys. Med. Biol. 11, 225–238.

Fewell, T. R., Shuping, R. E., 1977. Photon energy distribution of some typical diagnostic X-ray beams. Med. Phys. 4, 187–197.

Gramsch, E., Lynn, K. G., Weber, M., DeChillo, B., Mc Williams, J. R., 1992. Silicon PIN photodetectors in high resolution nuclear spectroscopy. Nucl. Instrum. Meth. A 311, 529–538.

Hubbel, J. H., 1982. Photon mass attenuation and energy-absorption coefficients from 1 keV to 20 MeV. Int. J. Appl. Radiat. Isot. 33, 1269–1290.

Israel, H.l., Lier, D. W., Storm, E., 1971. Comparison of detectors used in measurements of 10 to 300 keV X-ray spectra. Nucl. Instrum. Meth. 91, 141–157.

O'Foghludha, F., Johnson, G. A., 1981. Voltage wave forms effects on output and penetration of W- and M_0-anode mammographic tubes. Phys. Med. Biol. 26, 303–991.

Pani, R., Laitano, R. F., Pellegrini, R., 1987. Diagnostic X-ray spectra measurements using a silicon surface barrier detector. Phys. Med. Biol. 32, 1135–1149.

Rens, V., Westneier, W., 1983. Catalog of γ-rays from radioactive decay, Part II. Atomic Nucl. Data Tables 29, 193–406.

Sakai, E., 1987. Recent measurements of scintillator-photo detectors systems. IEEE Trans. Nucl. Sci. 34, 418–422.

Seelentag, W. W., Panzer, W., 1979. Stripping of X-ray Bremsstrahlung spectra up to 300 kVp on a desk type computer. Phys. Med. Biol. 24, 767–780.

Storm, E., Israel, H. I., 1970. Photon cross sections from 1 keV to 100 MeV for elements $Z = 1$ to $Z = 100$. Nucl. Data Tables A 7, 565–681.

Suffert, M., 1992. Silicon photodiode readout of scintillators and associated electronics. Nucl. Instrum. Meth. A 322, 528–532.

Tucker, D. M., Barnes, G. T., Chakraborty, D. P., 1991. Semiempirical model for generating tungsten target X-ray spectra. Med. Phys. 18, 211–218.

Yamamoto, H., Hatakeyama, S., Norimura, T., Tsuchiya, T., 1989. Low-energy nuclear radiation detection with a silicon photodiode. Nucl. Instrum. Meth. A 281, 128–132.

Appendix A

FLOW CHART OF PROGRAM FOR THE STRIPPING OF γ– AND X–RAYS SPECTRA MEASURED WITH PIN PHOTODIODE.